Premelting Behavior of a Langmuir−Blodgett Film of Dioctadecyldimethylammonium-Au(dmit)$_2$ Salt

Shin-ichi Morita,*,† Akifumi Ikehata,‡ Yasuhiro F. Miura,† Michio Sugi,† and Yukihiro Ozaki‡

Department of Functional Chemistry, Faculty of Engineering, Toin University of Yokohama, 1614 Kurogane-cho, Aoba-ku, Yokohama 225-8502, Japan, and Department of Chemistry, School of Science and Technology, Kwansei Gakuin University, 2-1 Gakuen, Sanda, Hyogo 669-1337, Japan

Received: May 31, 2004; In Final Form: August 10, 2004

Premelting behavior of a Langmuir−Blodgett (LB) film of dioctadecyldimethylammonium-Au(dmit)$_2$ ($2C_{18}$−Au(dmit)$_2$) salt has been studied by means of infrared (IR) transmission spectroscopy. Two bands due to the CH_2 antisymmetric stretching ($\nu_{as}(CH_2)$) and symmetric stretching ($\nu_s(CH_2)$) modes have been used to monitor the conformation and orientation of a hydrocarbon chain in the $2C_{18}$−Au(dmit)$_2$ LB film, and a band due to the C═S stretching mode has been employed to investigate the aggregation state of Au(dmit)$_2$ chromophores. The global phase mapping method in the generalized two-dimensional correlation spectroscopy (global 2D phase mapping method) has been used for examining the overlapping, shifting, and broadening of absorption components in the $\nu_s(CH_2)$ band (2841−2856 cm^{-1} region). Temperature-dependent IR spectral changes have revealed that there are, at least, four different ordered stages in the LB film below the order−disorder transition between 105 and 110 °C. (i) In the temperature range of 30−50 °C, the orientation and conformation of hydrocarbon chain and the aggregation state of Au(dmit)$_2$ chromophores do not change appreciably, in which the hydrocarbon chain contains the disordered component to some extent, compared to the most highly ordered state of the hydrocarbon chain at 60 °C. (ii) From 50 to 60 °C, the new aggregation state of Au(dmit)$_2$ chromophores appears, while the hydrocarbon chain changes drastically to the specific orientation where the transition moment of the $\nu_s(CH_2)$ mode tends to be aligned parallel to the substrate surface, with the trans forms increasing. (iii) From 60 to 80 °C, the aggregation state of Au(dmit)$_2$ chromophores observed at 30 °C is almost completely converted into the new aggregation state, while the hydrocarbon chain keeps the specific orientation on average, with the gauche forms increasing. (iv) From 80 to 105 °C, the new aggregation state of Au(dmit)$_2$ chromophores remains almost unchanged until the order−disorder transition, while the hydrocarbon chain changes to the disordered state, with the gauche forms increasing. The above results have indicated that the heat treatments after the film deposition can be used for controlling the structure of the $2C_{18}$−Au(dmit)$_2$ LB film.

Introduction

A great deal of attention has been paid to the fabrication of Langmuir−Blodgett (LB) films because the LB method is one of the best techniques for preparing highly oriented ultrathin films with structures controllable at the molecular level.[1−3] We have reported that an LB film of dioctadecyldimethylammonium-Au(dmit)$_2$ salt ($2C_{18}$−Au(dmit)$_2$ salt, Figure 1) shows a conductivity as high as 2 Scm^{-1} after electrochemical oxidation,[4] and our recent interest lies in the realization of the higher conductivity of the LB system using thermal treatments.

So far, thermal behavior of various kinds of LB films has been extensively studied.[5−10] For instance, thermal expansion coefficients of the LB films of cadmium salts of long chain fatty acids were estimated by X-ray diffraction analysis;[5] order−disorder transitions of those Cd salt LB films were investigated using infrared (IR) spectroscopy[6] and X-ray diffraction analysis;[7] thermal behavior of functional LB films was studied using IR and ultraviolet−visible spectroscopies, in which the aggregation states of functional dyes are related to the thermal motion of the hydrocarbon chain.[8−10]

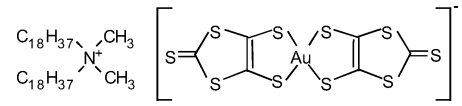

Figure 1. Chemical structure of the $2C_{18}$−Au(dmit)$_2$ salt.

We have investigated the premelting behavior of the $2C_{18}$−Au(dmit)$_2$ LB film in the heating process by means of IR spectroscopy. The global 2D phase mapping method in the generalized two-dimensional correlation spectroscopy (global 2D phase mapping method), which was previously proposed by our research groups for extracting the physical or chemical information more effectively from the perturbation-dependent IR spectra of functional LB films,[11−13] has been used for examining the overlapping, shifting, and broadening of absorption components in the CH_2 symmetric stretching ($\nu_s(CH_2)$) band region. The changes in the temperature-dependent IR spectra of the $2C_{18}$−Au(dmit)$_2$ LB film have revealed that there are at least four different ordered stages in the LB film below the order−disorder transition, indicating that the structure of the $2C_{18}$−Au(dmit)$_2$ LB film can be controlled by thermal treatments.

* To whom correspondence should be addressed. Tel: +81-45-972-5881. Fax: +81-45-972-5972. E-mail: smorita@cc.toin.ac.jp.
† Toin Univesity of Yokohama.
‡ Kwansei Gakuin University.

10.1021/jp040403b CCC: $27.50
Published on Web 11/19/2004

Experimental Section

The $2C_{18}-Au(dmit)_2$ salt was synthesized following the procedure by G. Steimecke et al.[14] For estimating the melting point of the bulk crystalline $2C_{18}-Au(dmit)_2$ salt, differential thermal analysis was carried out using a Rigaku Thermo Plus TG8120. The $2C_{18}-Au(dmit)_2$ salt was dissolved in a 1:1 mixture of benzene and acetonitrile (0.25 mM). The solution was spread on the surface of pure water prepared using a Milli-Q SP reagent water system (Millipore Corporation). The resistivity was larger than 1.8×10^7 Ωcm. The as-spread floating film of the salt was kept on the water surface for 5 min. The floating film was then compressed at a speed of 0.067 $Å^2$ $(molecule \cdot s)^{-1}$ up to 25 mNm^{-1} at 17 °C using a NIMA type 622 trough. A Teflon sheet with twelve rectangular windows (the thickness of the sheet: 2 mm, the size of each window: 41 × 21 mm) was put on the frame of the trough. The floating film in each window was then transferred onto a CaF_2 substrate (40 × 20 × 1 mm) by the horizontal lifting method. Twenty-layered LB films were deposited on one side of CaF_2 substrates for the IR and ultraviolet−visible spectroscopic measurements. We previously confirmed the reproducible film deposition up to 20 layers using ultraviolet−visible spectroscopy.[4] We also confirmed by means of atomic force microscopy that the $2C_{18}-Au(dmit)_2$ LB film transferred by a single deposition actually has a quasi three-dimensional structure.[15]

IR transmission absorption spectra were measured at a 4 cm^{-1} resolution using a Nicolet Magna 550 FT-IR spectrometer equipped with an MCT detector. To generate spectra with a high signal-to-noise ratio, 256 interferograms were coadded. For measuring temperature-dependent IR spectra, the CaF_2 substrate covered with the LB film was inserted into a metal holder with a metal heater and a thermocouple, each connected with a temperature controlling system, an Omron E5T. Ultraviolet−visible absorption spectra were measured using a Shimadzu UV-3101PC spectrometer.

Global 2D Phase Mapping Method

Calculation of a Global 2D Phase Map. In the present study, the global 2D phase mapping method in the generalized two-dimensional correlation spectroscopy (global 2D phase mapping method) is used for examining the overlapping, shifting, and broadening of the absorption components in the $\nu_s(CH_2)$ band (2841−2864 cm^{-1} region). The global 2D phase mapping method was proposed in previous publications.[11−13] The calculation of the global 2D phase map is based on the theoretical framework and the computational method of the generalized 2D correlation spectroscopy proposed by I. Noda.[16,17] The computational method for obtaining the synchronous and asynchronous functions, proposed by I. Noda,[16,17] is summarized in the Appendix. The generalized 2D synchronous and asynchronous maps were calculated using software called "2D-Pocha" developed by D. Adachi (Kwansei Gakuin University). The generalized 2D phase maps were calculated in Microsoft Excel 97 with data sets exported from 2D-Pocha.

Let $f(\nu, t_j)$ be the original spectrum at the wavenumber position ν and the temperature t_j as follows:

$$f(\nu, t_j) \equiv f_j(\nu) \qquad j = 1, 2, 3....m$$

We assume that only one band exists in the spectra $f_j(\nu)$, since the main purpose of the proposed method is to examine whether an apparent band shift is composed of the real shift of a single absorption component or the overlap of two or more absorption components. Note that, even if two or more absorption components exist overlapping with each other, they are treated as a "single band."

If a band shifts or broadens with its peak height changing as a function of temperature t_j, there often arises such a situation that some temperature-dependent profiles show the increasing tendencies while the others show the decreasing tendencies. In such a situation, the saturation of the global phase angle of ±90 degrees is observed in the global 2D phase map, which prevents us from analyzing the detailed pattern that reflects the band shifting or broadening phenomena.[13] The spectra $f_j(\nu)$, therefore should be transformed to proper spectra $y_j(\nu)$ by the normalization and scaling operation to visualize the patterns for the band shifting and broadening phenomena.

Based on the original spectrum $f_j(\nu)$, the normalized spectrum $g_j(\nu)$ is given by

$$g_j(\nu) = \frac{f_j(\nu)}{p_j} \tag{1}$$

where p_j corresponds to the maximum value in the spectrum $f_j(\nu)$ at the temperature t_j. The next step is the scaling operation given by

$$y_j(\nu) = \frac{j}{m} \cdot g_j(\nu) \tag{2}$$

For a spectrum $y_j(\nu)$, the global 2D phase map is given by

$$\Theta(\nu_1,\nu_2) = \arctan\left\{\frac{\Psi(\nu_1,\nu_2)}{\Phi(\nu_1,\nu_2)}\right\} \tag{3}$$

where $\Phi(\nu_1,\nu_2)$ and $\Psi(\nu_1,\nu_2)$ are the synchronous and asynchronous functions, respectively (as for the procedure for obtaining the functions $\Phi(\nu_1,\nu_2)$ and $\Psi(\nu_1,\nu_2)$, see Appendix). The synchronous function, $\Phi(\nu_1,\nu_2)$, contains the information on the identity of the waveforms of the temperature-dependent signal profiles at spectral positions ν_1 and ν_2; the asynchronous function, $\Psi(\nu_1,\nu_2)$, contains the information on the difference of the waveforms. Note that the practical calculation of the generalized 2D asynchronous map is based on the Hilbert transformation because of the computational efficiency, although the original theoretical framework of the generalized 2D correlation spectroscopy is based on the Fourier transformation.[17] For the general use of the global 2D phase map, the signal filtering method to mask the amplified noises in the baseline region was proposed,[11] although it is not used in the present study.

Simulation. Figures 2 and 3 summarize the simulated spectra in the typical cases and the corresponding patterns appearing in the global 2D phase map. An absorption component in temperature-dependent spectra can be represented by a Gaussian function as

$$y_j(\nu) = \frac{j}{m} \cdot \left[\exp\left\{\frac{\left(\nu + \alpha \cdot \frac{j-1}{m-1}\right)^2}{\left(w_0 + \beta \cdot \frac{j-1}{m-1}\right)^2} \cdot 4 \ln 2\right\}\right]^{-1} \qquad j = 1,2,3...m \tag{4}$$

where w_0 corresponds to an initial value of the full width of half-height, and α and β are so set that the Gaussian function shifts and broadens linearly as a function of the index j (temperature t_j).

In the simplest case where the peak height of an absorption component changes with the index j ($m = 11$, $w_0 = 10$, $\alpha = \beta$

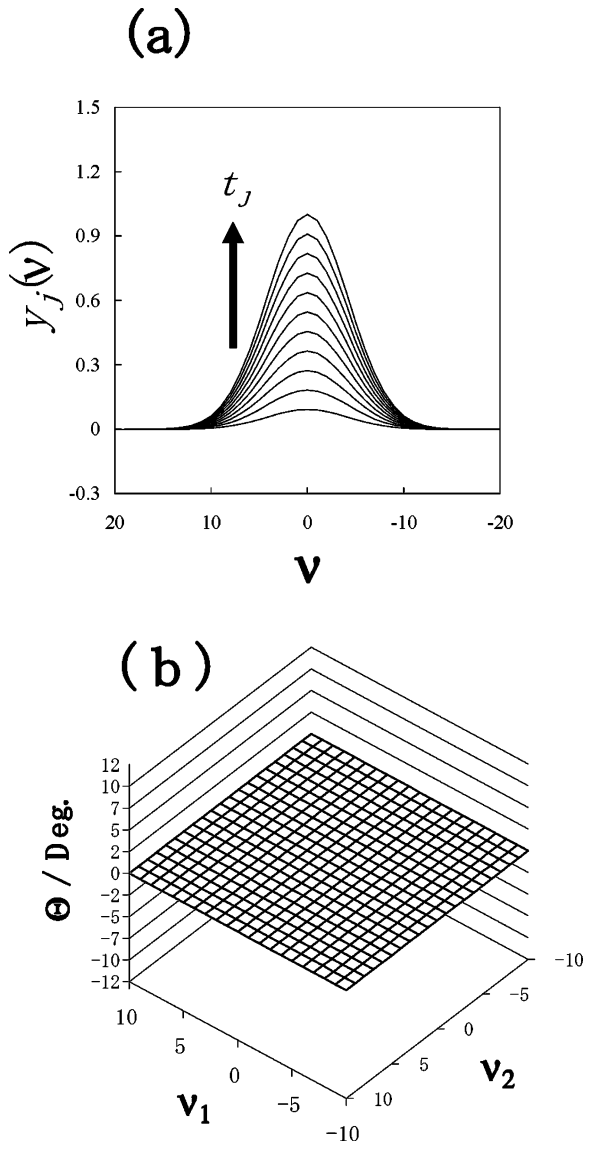

Figure 2. (a, b) Simulated spectra $y_j(\nu)$ at the temperature t_j and the spectral position ν, in the simplest case where the peak value of an absorption component increases linearly with temperature t_j and the corresponding global 2D phase map.

$= 0$), the auto correlation plane in the global 2D phase map shows a flat structure (Figure 2a,b). This is because the information of amplitude in the 1D spectra is canceled by eq 3.

On the other hand, the correlation plane in the global 2D phase map is subjected to a deformation when the absorption component shifts or broadens with the index j. The temperature-dependent change in the peak position of the absorption component ($m = 11$, $w_0 = 10$, $\alpha = 1$, $\beta = 0$) causes a tilted-structure in the global 2D phase map (Figure 3a,b); the temperature-dependent change in the width of the absorption component ($m = 11$, $w_0 = 8$, $\alpha = 0$, $\beta = 5$) generates a saddle-like structure (Figure 3c,d). Note that the change in the sign of α or β corresponds to the change in the sign of the global phase angle values.

Results and Discussion

Temperature-Dependent IR Spectra of a $2C_{18}-Au(dmit)_2$ LB Film. Figure 4 shows temperature-dependent IR transmission spectra (for the heating process) of a $2C_{18}-Au(dmit)_2$ LB film, where (a) and (b) refer to the regions of 2800−3000 cm^{-1} and 1000−1100 cm^{-1}, respectively. The baseline of each

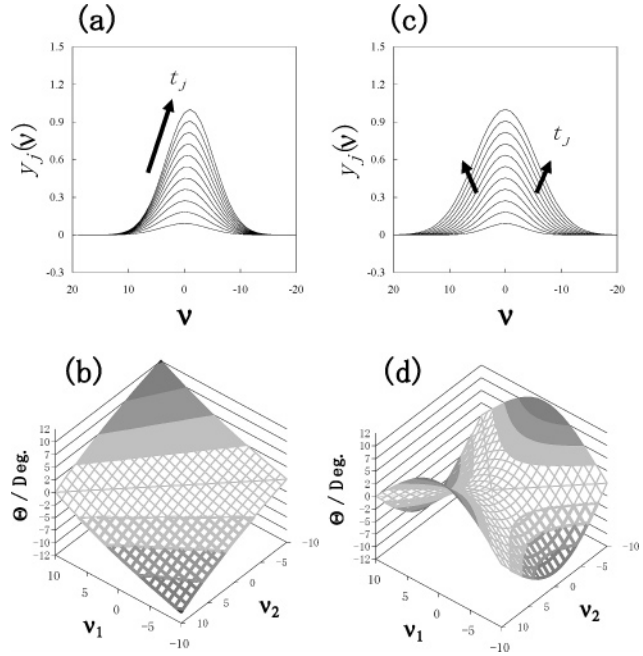

Figure 3. (a, b) Simulated spectra $y_j(\nu)$ at the temperature t_j and the spectral position ν, in which an absorption component shifts linearly with temperature t_j and the corresponding global 2D phase map. (c, d) Spectra $y_j(\nu)$ in which an absorption component broadens linearly with temperature t_j and the corresponding global 2D phase map.

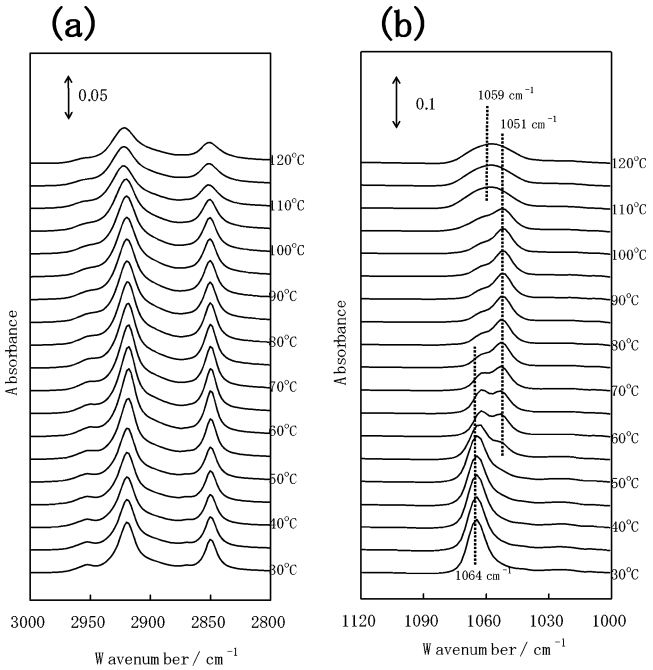

Figure 4. (a) Temperature-dependent IR transmission spectra of the $2C_{18}-Au(dmit)_2$ LB film (for the heating process) in the region of 2800−3000 cm^{-1}. The bands at 2920 and 2850 cm^{-1} are due to the CH_2 antisymmetric stretching ($\nu_{as}(CH_2)$) mode and the CH_2 symmetric stretching ($\nu_s(CH_2)$) mode, respectively. (b) Corresponding spectra in the region of 1000−1100 cm^{-1}. The band observed at around 1059 cm^{-1} is assigned to the C═S stretching mode.

spectrum was corrected by fitting a linear function, with the baseline region automatically selected using Grams/386 software, Galactic Industries Corporation. Note that, the offsets of the spectra in the figure were arbitrarily adjusted to distinguish the spectra from one another.

In Figure 4a, bands at 2920 and 2850 cm^{-1} are due to the CH_2 antisymmetric stretching ($\nu_{as}(CH_2)$) and symmetric

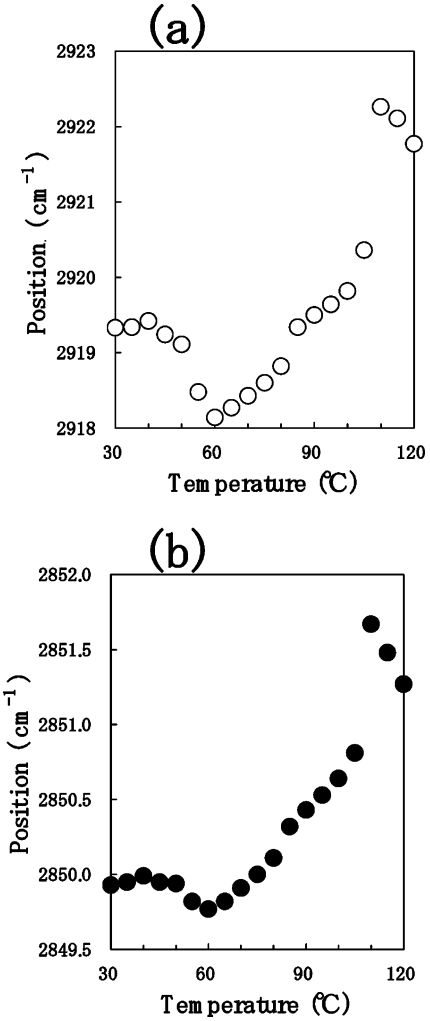

Figure 5. (a) Peak position of the $\nu_{as}(CH_2)$ band in Figure 4a. (b) Peak position of the $\nu_s(CH_2)$ band in Figure 4a.

stretching ($\nu_s(CH_2)$) modes, respectively. In Figure 4b, the absorption components observed at around 1059 cm^{-1} are assigned to the C═S stretching mode.[14,15] The C═S stretching band splits into the two absorption components at 1064 and 1051 cm^{-1} in the temperature range of 30−105 °C, and it becomes a single broad feature at 1059 cm^{-1} above 110 °C. So far, the origin of the split has not been identified. In both Figure 4a and Figure 4b, each spectrum changes drastically between 105 and 110 °C, indicating that an order−disorder transition occurs in the LB film. This is consistent with the melting point of 108.5 °C found for the bulk crystalline $2C_{18}-Au(dmit)_2$ salt.

Figure 5a,b shows the temperature-dependent peak positions of the $\nu_{as}(CH_2)$ and $\nu_s(CH_2)$ bands in Figure 4a, respectively. The peak positions in Figure 5a,b show nearly the same profile to each other. As is well known, the peak positions of the ν_{as}-(CH_2) and $\nu_s(CH_2)$ bands are sensitive to the conformation of hydrocarbon chains.[18,19] For example, when a hydrocarbon chain is in a solid crystalline state with all-trans conformation, the peaks of the $\nu_{as}(CH_2)$ and $\nu_s(CH_2)$ bands appear at around 2918 and 2848 cm^{-1}, respectively; when the hydrocarbon chain is in a liquid (isotropic) state where it contains the gauche forms, the peaks appear at around 2926 and 2856 cm^{-1}. The peak positions are therefore found to be useful indicators of the conformational change in the hydrocarbon chain. The peaks of these bands shift drastically to the higher wavenumber positions with increasing temperature from 105 to 110 °C, indicating the order−disorder transition of the LB film. The peaks shift apparently below the order−disorder transition of the LB film: between 30 and 50 °C, the peak positions of these two bands do not change appreciably; from 50 to 60 °C, they shift to the lower wavenumber positions; from 60 to 105 °C, they shift upward gradually.

For examining the overlapping, shifting, and broadening of absorption components in the $\nu_s(CH_2)$ band region, the global phase mapping analysis in the generalized two-dimensional correlation spectroscopy (global 2D phase mapping analysis) has been applied. Here, the $\nu_s(CH_2)$ band is intensively studied by the global 2D phase mapping analysis. This is because the $\nu_s(CH_2)$ band does not interfere with a band due to any other vibrational mode, while the $\nu_{as}(CH_2)$ band interferes with other vibrational bands. Figure 6a-d shows the global 2D phase maps calculated from the IR spectra in the $\nu_s(CH_2)$ band region of 2841−2864 cm^{-1} (corresponding to the spectra in Figure 4a). They refer to the temperature ranges of (a) 30−50 °C; (b) 40−60 °C; (c) 60−80 °C; (d) 85−105 °C, respectively. In each temperature range, the spectrum $f_j(\nu)$ is transformed to the corresponding spectrum $y_j(\nu)$ through the scaling operation (eqs 1, 2), for visualizing the characteristic patterns.

The pattern given in Figure 6a shows a flat structure, which agrees with the result that the peak position of the $\nu_s(CH_2)$ band remains almost unchanged in the temperature range of 30−50 °C (Figure 5b). The pattern observed in Figure 6b is composed of a tilted-structure at 2856 cm^{-1} and a saddle-like structure at 2848 cm^{-1}. These indicate that the peak of the absorption component at 2856 cm^{-1} due to the $\nu_s(CH_2)$ mode shifts to the lower wavenumber position, and that the absorption component at 2848 cm^{-1} due to the same vibrational mode narrows in the heating process of 40−60 °C. The pattern in Figure 6c consists of a flat structure at 2860 cm^{-1} and a saddle-like structure at 2848 cm^{-1}. These indicate that the component at 2860 cm^{-1} neither shifts nor broadens and that the component at 2848 cm^{-1} broadens in the heating process of 60−80 °C. The pattern in Figure 6d is also composed of a flat structure at 2860 cm^{-1} and a saddle-like structure at 2848 cm^{-1}, indicating that the component at 2860 cm^{-1} neither shifts nor broadens, and that the component at 2848 cm^{-1} broadens in the heating process of 85−105 °C. It should be noted that Figure 6d shows the more prominent saddle-like structure, compared to that in Figure 6c. This suggests that the component at 2848 cm^{-1} broadens more markedly in the temperature range of 85−105 °C than in the range of 60−80 °C.

The above global 2D phase mapping analysis has revealed that the band at 2850 cm^{-1} is composed of the major component at 2848 cm^{-1} and the minor component at 2856 cm^{-1}, and that the major component does not shift appreciably in the heating process of 30−105 °C. These indicate that the apparent shifts of the $\nu_s(CH_2)$ band observed in Figures 4a and 5b are mainly caused by the changes in the peak position and height of the minor component at 2856 cm^{-1}, although the minor component in itself can hardly be recognized with the naked eye, overlapping with the large slope of the major component at 2848 cm^{-1} (Figure 4a). Note that the absorption component at 2856 cm^{-1} observed in Figure 6b and that at 2860 cm^{-1} in Figure 6c,d are treated as one and the same component at 2856 cm^{-1}.

The difference in the frequencies of the major and minor components (2848 and 2856 cm^{-1}) is caused by the trans and gauche forms in the hydrocarbon chain, respectively.[18,19] For the major component at 2848 cm^{-1}, the narrowing and broadening phenomena recognized in the global 2D phase maps may be induced by the changes in the mobility and order of the hydrocarbon chain.

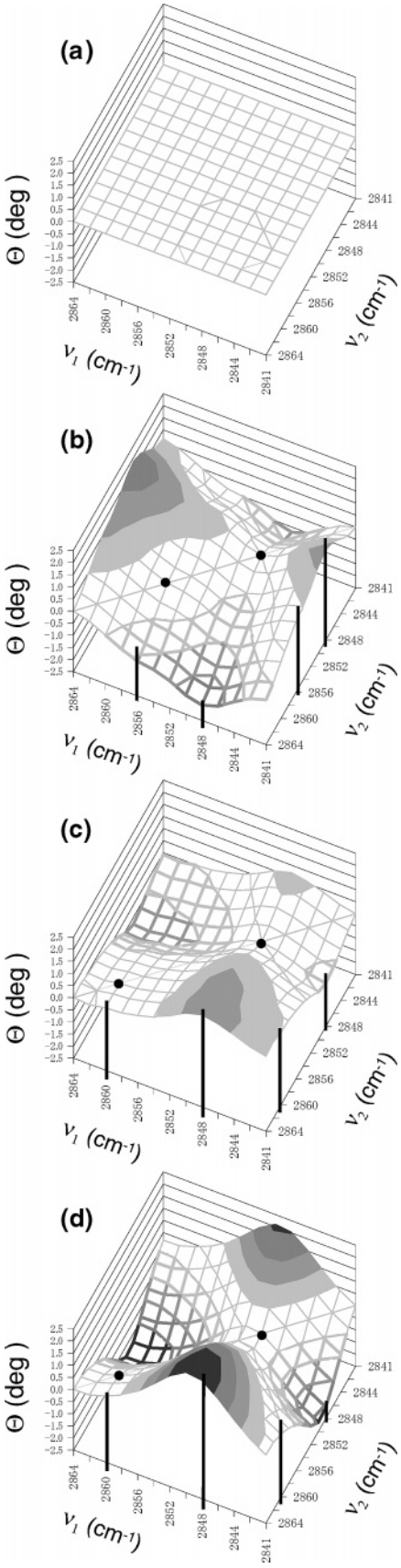

Figure 6. Global 2D phase maps calculated from the IR spectra for the $\nu_s(CH_2)$ region in the different temperature ranges: (a) 30−50 °C; (b) 40−60 °C; (c) 60−80 °C; (d) 85−105 °C.

In the heating process of 40−60 °C, the lower wavenumber shift of the minor absorption component at 2856 cm^{-1} is

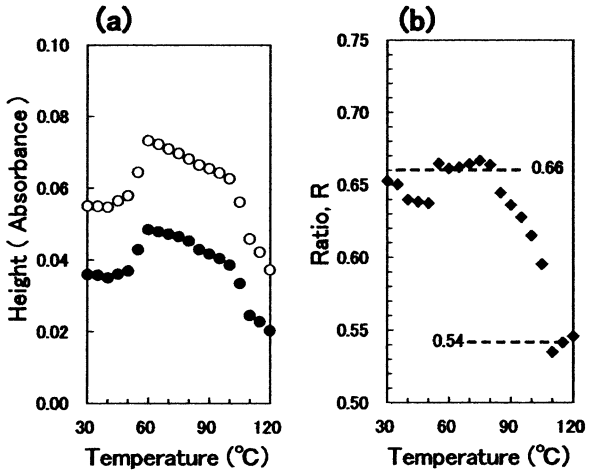

Figure 7. (a) Temperature-dependent peak height of the $\nu_{as}(CH_2)$ band (open circle, ○) and that of the $\nu_s(CH_2)$ band (solid circle, ●) in Figure 4a. (b) Ratio of the peak values in (a): the peak height of the $\nu_{as}(CH_2)$ band to that of the $\nu_s(CH_2)$ band.

detected using the global 2D phase mapping analysis (Figure 6b). Although we do not have so far any clear-cut explanation about the mechanism of the shift, the shift may be related to the change into the packing density of the hydrocarbon chains (to be mentioned below, in the heating process of 50−60 °C, the hydrocarbon chain, which contains the disordered component to some extent, changes drastically to the most highly ordered state with the specific orientation, which probably causes the change in the packing density of the hydrocarbon chains.)

Figure 7a shows peak heights of the $\nu_{as}(CH_2)$ and $\nu_s(CH_2)$ bands in Figure 4a as functions of temperature. In our optical system, we observe only the component of a transition moment parallel to the substrate surface, since the electric vector of incident IR light is parallel to a substrate surface. The maximum peak values of the $\nu_{as}(CH_2)$ and $\nu_s(CH_2)$ bands can be observed when a hydrocarbon chain is in the all-trans conformation with its long axis perpendicular to the substrate surface, because the direction of the long axis, and the transition moments of the $\nu_{as}(CH_2)$ and $\nu_s(CH_2)$ modes are perpendicular to one another. In the temperature range of 30−50 °C, the peak heights of the two bands do not change appreciably; from 50 to 60 °C, they increase markedly; from 60 to 105 °C, they decrease gradually; between 105 and 110 °C, they decrease rapidly.

Figure 7b shows the ratio of the peak values in Figure 7a as a function of temperature: the peak height of the $\nu_s(CH_2)$ band to that of the $\nu_{as}(CH_2)$ band. As mentioned above, the LB film is in the isotropic state between 110 and 120 °C. This indicates that the ratio of 0.54, which is observed between 110 and 120 °C, can be used as an approximate standard value for the isotropic orientation of the hydrocarbon chain. We assume that the major and minor components of the $\nu_s(CH_2)$ band recognized in Figure 6b−d share the same absorption coefficient. In the heating process of 30−105 °C, the ratio is larger than 0.54, indicating that the hydrocarbon chain has the specific orientation where the transition moment of the $\nu_s(CH_2)$ mode tends to be aligned parallel to the substrate surface. The maximum value of 0.66 is observed between 55 and 80 °C, and the other ratios show the intermediate values between 0.66 and 0.54. These indicate that, between 55 and 80 °C, the hydrocarbon chain is in the most highly ordered state with the specific orientation, and that, in the other temperature ranges (30−50 °C and 85−105 °C), the hydrocarbon chain contains the disordered component to some extent, compared to the most highly ordered state of the hydrocarbon chain between 55 and 80 °C. Further

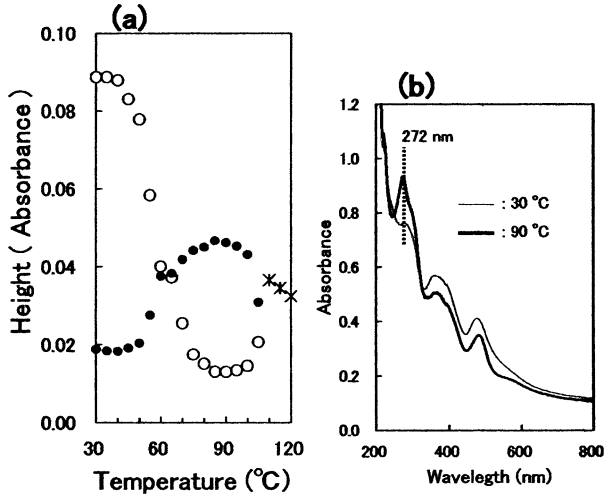

Figure 8. (a) Temperature-dependent peak heights of the absorption components due to the C═S stretching mode in Figure 4b. The overlapped band at around 1060 cm^{-1} between 30 and 105 °C in Figure 4b is separated into the absorption component at around 1064 (open circle, ○) and the component at around 1051 cm^{-1} (solid circle, ●) using the curve fitting method. The peak height of the band above 110 °C is regarded as the single absorption component (asterisk). (b) Ultraviolet−visible spectra of the $2C_{18}-Au(dmit)_2$ LB film at 30 and 90 °C.

details of the conformation and orientation changes in the hydrocarbon chain are given in the following section.

Figure 8a shows peak heights of the absorption components due to the C═S stretching mode as functions of temperature in Figure 4b. The global 2D phase mapping analysis is not applied to this case, since the two absorption components at around 1060 cm^{-1} between 30 and 105 °C (Figure 4b) can easily be recognized. The overlapped band is eventually separated into the two components at 1064 and 1051 cm^{-1} using the curve fitting method (in Grams/386 software, Galactic Industries Corporation). From 30 to 50 °C, the peak height of the major component at 1064 cm^{-1} remains almost unchanged but, from 50 to 80 °C, it decreases drastically and the peak height of the component at 1051 cm^{-1} increases instead. From 80 to 105 °C, the peak height of the major component at 1051 cm^{-1} remains nearly unchanged. Between 105 and 110 °C, the component at 1052 cm^{-1} disappears and turns into the broad single component at 1059 cm^{-1}.

It should be noted that the two profiles in the temperature range of 30−105 °C are closely correlated with each other as seen in Figure 8a, with the correlation coefficient of −0.967 (−0.996 in case of 30−100 °C). We consider that the correlation coefficient close to −1 reflects the shift in the equilibrium between the two different aggregation states of $Au(dmit)_2$ chromophores by heating, and that the aggregation state of $Au(dmit)_2$ chromophores observed at 30 °C is probably converted to a new aggregation state above 80 °C. In fact, an ultraviolet−visible spectrum of the LB film at 90 °C shows a characteristic sharp band at 272 nm, while the corresponding band at 30 °C is, in contrast, far less prominent: lower in height and more diffuse in sharpness (see Figure 8b). It is therefore indicated that the aggregation state of $Au(dmit)_2$ chromophores at 90 °C is distinct from that at 30 °C.

Premelting Behavior of the $2C_{18}-Au(dmit)_2$ LB Film. The premelting behavior of the $2C_{18}-Au(dmit)_2$ LB film is now described based on the results given in the preceding section. In the heating process, four different ordered stages have been recognized in the $2C_{18}-Au(dmit)_2$ LB film below the order−disorder transition between 105 and 110 °C. They can be categorized as follows. (i) In the heating process of 30−50 °C, the conformation and orientation of hydrocarbon chain and the aggregation state of $Au(dmit)_2$ chromophores do not change appreciably. The hydrocarbon chain contains the disordered component to some extent, compared to the most highly ordered state of the hydrocarbon chain at 60 °C. (ii) In the heating process of 50−60 °C, the orientation of hydrocarbon chain changes drastically so that the transition moments of the $\nu_{as}(CH_2)$ and $\nu_s(CH_2)$ modes approach the direction parallel to the substrate surface, increasing the trans forms. The hydrocarbon chain reaches the most highly ordered state with the specific orientation at 60 °C, in which the transition moment of the $\nu_s(CH_2)$ mode tends to be aligned parallel to the substrate surface, and a new aggregation state of $Au(dmit)_2$ chromphores appears. (iii) From 60 to 80 °C, the hydrocarbon chain keeps the specific orientation on average, with the gauche forms increasing. The aggregation state of $Au(dmit)_2$ chromphores at 30 °C is converted almost completely into the new aggregation state at 80 °C. (iv) From 80 to 105 °C, the hydrocarbon chain changes into the disordered state, with the gauche forms increasing. The new aggregation state of $Au(dmit)_2$ chromphores remains almost unchanged until the order−disorder transition of the LB film.

Conclusion

The premelting behavior of the hydrocarbon chain and the chromophore of the $2C_{18}-Au(dmit)_2$ LB film has been studied by means of IR transmission spectroscopy. In the heating process, four different ordered stages have been recognized in the LB film below the order−disorder transition between 105 and 110 °C. The results are important, showing that the heat treatment can be a powerful and versatile tool to control the structure of the LB film. As mentioned in the Introduction, we have reported that the $2C_{18}-Au(dmit)_2$ LB film shows high in-plane conductivity of 2 Scm^{-1} after electrochemical oxidation, and our interest lies in the realization of higher conductivity of the same LB film system by means of the secondary treatments after the deposition. In this respect, the conductivity of the LB film after the heat treatment is now intensively studied in relation to the structure of the LB film, and the results will be reported elsewhere soon.

Acknowledgment. The authors are grateful to Mr. Ryo Watanabe and Dr. Yoshiaki Hirano (Faculty of Engineering, Toin University of Yokohama) for valuable discussions and technical assistance.

Appendix: Derivation of the Synchronous and Asynchronous Functions

For the spectrum $y_i(\nu)$ at the wavenumber position ν and the temperature t_j , the dynamic spectrum is defined by I. Noda[16] as follows:

$$\tilde{y}_j(\nu) = y_j(\nu) - \bar{y}(\nu) \tag{5}$$

As the reference spectrum in eq 5, the temperature-averaged spectrum is usually used; the spectrum is defined as

$$\bar{y}(\nu) = \frac{1}{m}\sum_{j=1}^{m} y_j(\nu) \tag{6}$$

The next step is the calculation of the generalized 2D synchronous and asynchronous maps, $\Phi(\nu_1, \nu_2)$ and $\Psi(\nu_1, \nu_2)$, which is proposed by I. Noda:[16,17]

$$\Phi(\nu_1,\nu_2) = \frac{1}{m-1}\sum_{j=1}^{m} \tilde{y}_j(\nu_1)\cdot\tilde{y}_j(\nu_2) \tag{7}$$

$$\Psi(\nu_1,\nu_2) = \frac{1}{m-1}\sum_{j=1}^{m} \tilde{y}_j(\nu_1)\cdot\tilde{z}_j(\nu_2) \tag{8}$$

where

$$\tilde{z}_j(\nu_2) = \sum_{k=1}^{m} N_{jk}\cdot\tilde{y}_k(\nu_2) \tag{9}$$

Here we recognize

$$N_{jk} = \begin{cases} 0 & \text{if } j = k \\ 1/\pi(k-j) & \text{otherwise} \end{cases} \tag{10}$$

References and Notes

(1) Kuhn, H. *Naturwissenschaften* **1967**, *54*, 429.
(2) Kuhn, H. *Thin Solid Films* **1989**, *178*, 1.
(3) Sugi, M. *J. Mol. Electron.* **1985**, *2*, 3.
(4) Miura, Y. F.; Kurashige, Y.; Hirano, Y.; Kawata, J.; Sugi, M. *Thin Solid Films* **1998**, *327*−*329*, 443.
(5) Fukui, T.; Sugi, M.; Iizima, S. *Phys. Rev. B* **1980**, *22*, 4898.
(6) Naselli, C.; Rabolt, J. F.; Swalen, J. D. *J. Chem. Phys.* **1985**, *82*, 2136.
(7) Sasanuma, Y.; Kitano, Y.; Ishitani, A.; Nakahara, H.; Fukuda, K. *Thin Solid Films* **1991**, *199*, 359.
(8) Fukui, T.; Saito, M.; Sugi, M.; Iizima, S. *Thin Solid Films* **1983**, *109*, 247.
(9) Liang, K.; Law, K. Y.; Whitten, D. G. *J. Phys. Chem.* **1994**, *98*, 13379.
(10) Wang, Y.; Nichogi, K.; Terashita, S.; Iriyama, K.; Ozaki, Y. *J. Phys. Chem.* **1996**, *100*, 368.
(11) Morita, S.; Ozaki, Y.; Noda, I. *Appl. Spectrosc.* **2001**, *55*, 1618.
(12) Morita, S.; Ozaki, Y.; Noda, I. *Appl. Spectrosc.* **2001**, *55*, 1622.
(13) Morita, S.; Ozaki, Y. *Appl. Spectrosc.* **2002**, *56*, 502.
(14) Steimecke, G.; Sieler, H. J.; Kirmse, P.; Hoyer, E. *Phosphorus Sulfur* **1979**, *7*, 49.
(15) Horikiri, M.; Miura, Y. F.; Araki, Y.; Ikegami, K.; Sugi, M. *Colloids Surf. A* **2002**, *198*−*200*, 657.
(16) Noda, I. *Appl. Spectrosc.* **1993**, *47*, 1329.
(17) Noda, I. *Appl. Spectrosc.* **2000**, *54*, 994.
(18) Umemura, J.; Cameron, D. G.; Mantsch, H. H. *Biochim. Biophys. Acta* **1980**, *602*, 32.
(19) Sapper, H.; Cameron, D. G.; Mantsch, H. H. *Can. J. Chem.* **1981**, *59*, 2543.